Monthly Notices
of the
ROYAL ASTRONOMICAL SOCIETY

MNRAS **473,** 4558–4565 (2018)
Advance Access publication 2017 October 9

doi:10.1093/mnras/stx2610

Shear and vorticity in the spherical collapse of dark matter haloes

Robert Reischke,[1]★ Francesco Pace,[2] Sven Meyer[3] and Björn Malte Schäfer[1]

[1]*Astronomisches Recheninstitut, Zentrum für Astronomie der Universität Heidelberg, Philosophenweg 12, D-69120 Heidelberg, Germany*
[2]*Jodrell Bank Centre for Astrophysics, School of Physics and Astronomy, The University of Manchester, Manchester M13 9PL, UK*
[3]*Institut für theoretische Astrophysik, Zentrum für Astronomie der Universität Heidelberg, Philosophenweg 12, D-69120 Heidelberg, Germany*

Accepted 2017 October 1. Received 2017 October 1; in original form 2016 December 14

ABSTRACT

Traditionally, the spherical collapse of objects is studied with respect to a uniform background density, yielding the critical overdensity δ_c as a key ingredient to the mass function of virialized objects. Here, we investigate the shear and rotation acting on a peak in a Gaussian random field. By assuming that collapsing objects mainly form at those peaks, we use this shear and rotation as external effects changing the dynamics of the spherical collapse, which is described by the Raychaudhuri equation. We therefore assume that the shear and rotation have no additional dynamics on top of their cosmological evolution and thus only appear as inhomogeneities in the differential equation. We find that the shear will always be larger than the rotation at peaks of the random field, which automatically results into a lower critical overdensity δ_c, since the shear always supports the collapse, while the rotation acts against it. Within this model, δ_c naturally inherits a mass dependence from the Gaussian random field, since smaller objects are exposed to more modes of the field. The overall effect on δ_c is approximately of the order of a few per cent with a decreasing trend to high masses.

Key words: methods: analytical – large-scale structure of Universe – cosmology: theory.

1 INTRODUCTION

The combined observations of Type Ia supernovae (e.g. Riess et al. 1998; Perlmutter et al. 1999), the cosmic microwave background (e.g. Komatsu et al. 2011; Planck Collaboration XIII 2016), the Hubble constant and large-scale structure (e.g. Cole et al. 2005) show that the Universe is spatially flat and expanding in an accelerated fashion. Under the assumptions of General Relativity being true and the symmetries of the Friedmann–Robertson–Walker metric, the accelerated expansion can be described by the cosmological constant Λ or by adding a fluid component (see e.g. Copeland, Sami & Tsujikawa 2006, for a review) to the energy-momentum content of the Universe with an equation of state $w < -1/3$ which may be time dependent. In this scenario, generally called dark energy, Λ would correspond to a constant $w = -1$.

The equation-of-state parameter, as well as the other parameters such as the dark energy content Ω_Λ or the matter content Ω_m of the cosmological standard model, can and already have been measured to very high precision. However, with high precision comes also the risk of possible biases in the parameters if the theoretical prediction and astrophysics are not modelled well enough. It is therefore necessary to review and perhaps modify common concepts and models since possible systematics are no longer wiped out by the statistical errors of the experiment.

★ E-mail: reischke@stud.uni-heidelberg.de

The halo mass function is, due to its exponential sensitivity, one of the main tools to provide robust theoretical predictions for many observables such as cluster counts (Sunyaev & Zeldovich 1980; Diego & Majumdar 2004; Majumdar 2004; Fang & Haiman 2007; Abramo, Batista & Rosenfeld 2009; Angrick & Bartelmann 2009) or weak lensing peak counts (Maturi et al. 2010; Maturi, Fedeli & Moscardini 2011; Lin & Kilbinger 2014; Reischke, Maturi & Bartelmann 2016b). As it deals with objects in the highly non-linear regime, one needs to extrapolate the linearly evolved density to the non-linear one which is encoded in the critical linear overdensity δ_c.

This can be done by using the spherical collapse model introduced by Gunn & Gott (1972) and later extended in several works (Fillmore & Goldreich 1984; Bertschinger 1985; Ryden & Gunn 1987; Avila-Reese, Firmani & Hernández 1998; Mota & van de Bruck 2004; Abramo et al. 2007; Pace, Waizmann & Bartelmann 2010; Pace et al. 2014a). This model assumes in its most simplistic form, called standard spherical collapse (SPC hereafter), the evolution of a spherically symmetric density perturbation in an expanding background with uniform background density, i.e. an isolated collapse. The overdensity grows until it reaches a critical point at which it starts to collapse under its own gravity. Due to the collapse, it decouples from the expansion. In theory, the overdense region would collapse to a single point, however, the energy released during the collapse is converted into random motions of the particles, such that an equilibrium situation (in the sense of a virialized structure; Schäfer & Koyama 2008) is created. Effectively,

© 2017 The Authors
Published by Oxford University Press on behalf of the Royal Astronomical Society

Downloaded from https://academic.oup.com/mnras/article-abstract/473/4/4558/4411833
by University of Manchester user
on 30 November 2017

we start from initial conditions such that such a virialized structure is formed at a certain redshift. These initial conditions are then used to propagate the linear growth of structures, described by the overdensity δ. The corresponding linear δ at the redshift where the non-linear solution resulted into a virialized object is then called δ_c. It therefore sets a threshold above which an object can be considered as being collapsed even in terms of linear structure formation. Given this value, one can predict the abundances of collapsed objects in terms of a random walk with a moving barrier.

It is necessary to check the validity of the SPC model and introduce additional effects subject to more realistic situations. One of the ingredients of the SPC model is the embedding of the spherical region into a uniform background. In this way, no external forces can act on the halo by virtue of Birkhoff's theorem. However, haloes are embedded in a random field giving rise to gravitational tidal fields inducing shear and rotation acting on the collapsing spherical region and thus changing the collapse dynamics.

In earlier works (Del Popolo, Pace & Lima 2013a,b; Pace, Batista & Del Popolo 2014b), the influence of rotation and shear has been studied extensively using a phenomenological model introducing an additional term to match the Newtonian predictions. The authors found that the effect of shear is always smaller than the effect of the rotation, leading to a slowdown of the collapse. Consequently, δ_c is larger compared to the SPC scenario, where it adopts the known value 1.686. The additional term has a mass dependence leading to a mass-dependent δ_c as well. Lower mass haloes are exposed to higher values of rotation and shear, leading to a higher δ_c while it becomes negligible for haloes with $M \gtrsim 10^{15}\,\mathrm{M}_\odot$.

More recently, Reischke et al. (2016a, hereafter R16) investigated a test particle embedded in tidal gravitational fields described by a Gaussian random field. The Gaussian random field obeys the statistics of the cosmic density field δ by virtue of the Zel'Dovich approximation (Zel'Dovich 1970). This gives rise to an effective shear acting on the collapsing region. The mass dependence of the shear is introduced naturally by assigning a length-scale to an object of mass M. Since the shear is treated as a random variable, δ_c is a random variable as well and has a distribution rather than a distinct value and the averaged value should be used for the mass function. It was shown in R16 that the effect on δ_c can cause a 1σ bias in cosmological parameters when considering an idealized cluster survey. Pace et al. (2017) studied the effect of shear in clustering dark energy models, finding similar results to the smooth case.

Since the tidal field examined in R16 is described by a potential flow, there is no vorticity generation. However, a rotation of the collapsing region can be modelled by a mechanism called tidal torquing (White 1984; Catelan & Theuns 1996; Crittenden et al. 2001; Schäfer 2009; Schäfer & Merkel 2012). We will therefore consider a peak in the density field with inertial tensor $\boldsymbol{I}$ and tidal shear tensor $\boldsymbol{\Psi}$ and investigate jointly the induced shear and rotation. Assuming that haloes form at peaks, we will use the values estimated for the shear and the rotation as an input for the spherical collapse model leading to a self-consistent description of the spherical collapse in gravitational tidal fields. We will furthermore show that the restriction to peaks in the density field has some very general consequences on the induced rotation and shear.

The structure of the paper is as follows. In Section 2, we very briefly review the spherical collapse model and show the equations to be solved. In Section 3, we introduce the statistical procedure to obtain tidal shear values and decompose them to identify the shear and rotation tensor, respectively. The obtained invariants are then used in Section 4 to calculate the influence of the tidal fields on δ_c for the standard ΛCDM model. We summarize our findings in Section 5.

2 SPHERICAL COLLAPSE

The spherical collapse model has been discussed by various authors, e.g. Bernardeau (1994), Padmanabhan (1996), Ohta, Kayo & Taruya (2003), Ohta, Kayo & Taruya (2004), Abramo et al. (2007) and Pace et al. (2010, 2014a), and its standard scenario describes the evolution of a spherical overdense region in an homogeneous expanding background. The key quantity derived from the spherical collapse is the critical overdensity δ_c which allows an extrapolation from the linear evolved density field to virialized structures. Therefore, δ_c is primal for the study of the abundance of objects in the Universe. Starting from the perturbed hydrodynamical equations

$$\begin{aligned} \dot{\delta} + (1+\delta)\nabla_{\boldsymbol{x}}\boldsymbol{u} &= 0, \\ \dot{\boldsymbol{u}} + 2H\boldsymbol{u} + (\boldsymbol{u}\cdot\nabla_{\boldsymbol{x}})\boldsymbol{u} &= -\frac{1}{a^2}\nabla_{\boldsymbol{x}}\phi, \\ \nabla^2_{\boldsymbol{x}}\phi &= 4\pi G a^2 \rho_0 \delta, \end{aligned} \tag{1}$$

with comoving coordinate $\boldsymbol{x}$, comoving peculiar velocity $\boldsymbol{u}$, Newtonian potential ϕ, overdensity δ and background density ρ_0, respectively. Here, the dot represents a derivative with respect to cosmic time t. Taking the divergence of the Euler equation and inserting the Poisson equation yields

$$\begin{aligned} \dot{\delta} &= -(1+\delta)\theta, \\ \dot{\theta} &= -2H\theta - 4\pi G\rho_0\delta - \frac{1}{3}\theta^2 - (\sigma^2 - \omega^2). \end{aligned} \tag{2}$$

Here, we used the decomposition

$$\nabla_{\boldsymbol{x}}\cdot[(\boldsymbol{u}\nabla_{\boldsymbol{x}})\boldsymbol{u})] = \frac{1}{3}\theta^2 + \sigma^2 - \omega^2, \tag{3}$$

with the expansion $\theta = \nabla_{\boldsymbol{x}}\cdot\boldsymbol{u}$, the shear $\sigma^2 \equiv \sigma_{ij}\sigma^{ij}$ and the rotation $\omega^2 \equiv \omega_{ij}\omega^{ij}$ assuming a spherical symmetry. The rotation and the shear tensors are themselves the antisymmetric and the symmetric traceless part of the velocity divergence tensor, respectively. They are defined as

$$\begin{aligned} \sigma_{ij} &= \frac{1}{2}\left(\partial_i u_j + \partial_j u_i\right) - \frac{\theta}{3}\delta_{ij}, \\ \omega_{ij} &= \frac{1}{2}\left(\partial_i u_j - \partial_j u_i\right), \end{aligned} \tag{4}$$

where $\partial_i \equiv \partial/\partial x^i$. We now use the relation $\partial_t = aH(a)\partial_a$ and $\tilde{\delta} = 1/\delta$ which leads to

$$\begin{aligned} \tilde{\delta}' &= \frac{\theta}{aH}\tilde{\delta}(1+\tilde{\delta}), \\ \theta' &= -\frac{2\theta}{a} - \frac{3H\Omega_{\mathrm{m}}}{2a\tilde{\delta}} - \left(\frac{1}{3}\theta^2 + \sigma^2 - \omega^2\right)\frac{1}{aH}, \end{aligned} \tag{5}$$

where the prime denotes a derivative with respect to a. The system defined in equation (5) is solved numerically until $\tilde{\delta} \sim 10^{-8}$ and then it is extrapolated to zero, which is much more stable than treating the system in δ rather than $\tilde{\delta}$. This yields the appropriate initial conditions for the linear version of equation (5) which gives δ_c. Usually σ^2 and ω^2 are neglected, however, their influence has phenomenologically been investigated, e.g. by Del Popolo et al. (2013a,b) in the ΛCDM and dark energy cosmologies and by Pace et al. (2014b) in clustering dark energy models. The authors heuristically model the term $\sigma^2 - \omega^2$ allowing us to study an isolated collapse including a (mass-dependent) quantity α, defined as the

Downloaded from https://academic.oup.com/mnras/article-abstract/473/4/4558/4411833
by University of Manchester user
on 30 November 2017

ratio between the rotational and the gravitational term. Specifically, the term is

$$\alpha = \frac{L^2}{M^3 RG}, \tag{6}$$

where L is the angular momentum of the spherical overdensity considered. M and R are its mass and radius, respectively. The angular momentum is important for galaxies, but negligible for clusters. In particular, $\alpha \approx 0.05$ for $M \approx 10^{11}\mathrm{M}_\odot h^{-1}$ and of the order of 10^{-6} for $M \approx 10^{15}\mathrm{M}_\odot h^{-1}$. By defining new quantities $\tilde{\theta} = \theta/H$, $\tilde{\sigma} = \sigma/H$ and $\tilde{\omega} = \omega/H$, the combined contribution of the shear and rotation term can effectively be modelled by

$$\tilde{\sigma}^2 - \tilde{\omega}^2 = -\frac{3}{2}\alpha\Omega_\mathrm{m}\delta, \tag{7}$$

leading to modified equations for the spherical collapse. Clearly $\tilde{\sigma}^2 - \tilde{\omega}^2$ is always negative, thus leading to a slowdown of the collapse. Technically, the term leads to larger initial conditions for the density contrast for a halo to be formed at a certain redshift, thus increasing δ_c as it is obtained from the linear equation using these initial conditions.

3 SHEAR AND ROTATION

3.1 The model

In this work, we intend to model the shear invariant σ^2, together with the rotation invariant ω^2, which occurs in the collapse equation (5). Earlier works studied the joint influence of shear and rotation in a phenomenological way as mentioned in the last section. The logic here is the following: we assume that dark matter haloes form at peaks of the density field, which itself is described by a Gaussian random field and thus by its power spectrum. In order to model $\sigma^2 - \omega^2$, we calculate these values at peaks of the density field using only the statistics of the field itself and the Zel'Dovich approximation. We then effectively place a test particle into the Gaussian random field at the peak and let it undergo a gravitational collapse, with the shear and rotation acting as external forces with no own dynamics (except for the ones given by the background dynamics). Thus, the collapse dynamics will stay spherical, while we allow for deviations from sphericity in the estimation of the shear and rotation (especially to find an expression for the inertial tensor). In this way, the collapsing object can be seen as a test particle in a tidal gravitational field.

3.2 The tidal tensor

The central object of our model is the tidal tensor $\mathbf{\Psi}$, which is related to the density field. For scales large enough, particles follow Zel'Dovich trajectories (Zel'Dovich 1970)

$$x_i = q_i - D_+(t)\partial_i\psi \equiv q_i - D_+(t)\psi_{,i}. \tag{8}$$

The displacement field ψ is related to the density contrast δ via a Poisson relation, $\Delta\psi = \delta$. In Fourier space, we can thus write the components of the tidal tensor as

$$\psi_{,ij} = -\int \frac{\mathrm{d}^3k}{(2\pi)^3}\frac{k_i k_j}{k^2}\delta(\boldsymbol{k})\exp(\mathrm{i}\boldsymbol{k}\boldsymbol{x}). \tag{9}$$

We now choose spherical coordinates in such a way that the peaks under consideration lie symmetric around the origin on the z-axis (Regős & Szalay 1995; Heavens & Sheth 1999). For convenience, we introduce dimensionless complex variables

$$y^n_{lm} = \sqrt{4\pi}\frac{\mathrm{i}^{l+2n}}{\sigma_{l+2n}}\int \frac{\mathrm{d}^3k}{(2\pi)^3}k^{l+2n}\delta(\boldsymbol{k})Y_{lm}(\hat{k})\exp(\mathrm{i}\boldsymbol{k}\boldsymbol{x}), \tag{10}$$

with the direction vector $\hat{k} = \boldsymbol{k}/k$ and σ_i being the spectral moments of the matter power spectrum

$$\sigma_i^2 = \frac{1}{2\pi^2}\int \mathrm{d}k\, k^{2i+2}P(k), \tag{11}$$

and Y_{lm} are the spherical harmonics. With this, we obtain a linear relation (Schäfer & Merkel 2012) between y^n_{lm} and the tidal field values $\psi_{,ij}$

$$\begin{aligned}
\sigma_0 y^{-1}_{20} &= -\sqrt{\frac{5}{4}}\left(\psi_{,xx} + \psi_{,yy} - 2\psi_{,zz}\right),\\
\sigma_0 y^{-1}_{2\pm1} &= -\sqrt{\frac{15}{2}}\left(\psi_{,xz} \pm \mathrm{i}\psi_{,yz}\right),\\
\sigma_0 y^{-1}_{2\pm2} &= \sqrt{\frac{15}{8}}\left(\psi_{,xx} - \psi_{,yy} \pm 2\mathrm{i}\psi_{,xy}\right),\\
\sigma_0 y^{0}_{00} &= \left(\psi_{,xx} + \psi_{,yy} + \psi_{,zz}\right).
\end{aligned} \tag{12}$$

The variables y^n_{lm} now have a diagonal autocorrelation matrix:

$$\left\langle y^n_{lm}(\boldsymbol{x})y^{n'}_{l'm'}(\boldsymbol{x})^*\right\rangle = (-1)^{n-n'}\frac{\sigma^2_{l+n+n'}}{\sigma_{l+2n}\sigma_{l+2n'}}\delta_{ll'}\delta_{mm'}. \tag{13}$$

By inverting the linear relation, we can draw random samples in the y^n_{lm} basis and calculate the components of the tidal tensor $\mathbf{\Psi}_{ij} \equiv \psi_{,ij}$. The strength of the tidal field depends on the characteristic length-scale $R(M)$ of the halo and thus on its mass. We thus introduce a low-pass filter to cut off high-frequency modes, suppressing fluctuations on scales smaller than the characteristic scale of the halo:

$$P(k) \rightarrow P(k)W_R^2(k), \tag{14}$$

with $W_R(k) = \exp(-k^2R^2/2)$. The mass scale is obtained via $M = \frac{4\pi}{3}\rho_\mathrm{crit}\Omega_\mathrm{m}R^3$, where $\rho_\mathrm{crit} = 3H^2/(8\pi G)$ is the critical density. For more details on the tidal field and the random process, we refer to R16.

3.3 Tidal torquing

Having presented the procedure to sample the components of the tidal tensor directly from the statistics of the density field, we introduce a mechanism known as tidal torquing in order to describe the generation of rotation due to tidal gravitational fields. In the picture of tidal torquing, angular momentum is generated by the tidal gravitational field which exerts a torquing moment on the halo. It is important to note that the vorticity $\boldsymbol{\omega}$ is not driven by the nonlinear term $\nabla\times(\boldsymbol{v}\times\boldsymbol{\omega})$ in the Euler equation. On the contrary, the angular momentum is generated by vorticity-free flows generating shear effects on the halo prior to collapse. During this process, the halo is slightly deformed and tends to align its inertia tensor in the eigenframe of the shear tensor. After decoupling from the shear flow and the start of collapse, the length of the lever arms reduces dramatically in comoving coordinates making tidal torquing inefficient. Therefore, the angular momentum just before collapse begins is a good proxy for the total rotation of the halo.

The angular momentum $\boldsymbol{L}$ of a rotating mass distribution $\rho(\boldsymbol{r}, t)$ is given by

$$\boldsymbol{L}(t) = \int_V \mathrm{d}^3r\,(\boldsymbol{r} - \bar{\boldsymbol{r}})\times\boldsymbol{v}(\boldsymbol{r}, t)\rho(\boldsymbol{r}, t), \tag{15}$$

Downloaded from https://academic.oup.com/mnras/article-abstract/473/4/4558/4411833
by University of Manchester user
on 30 November 2017

with $\boldsymbol{v}$ being the rotational velocity and V the physical volume under consideration. Making use of the Zel'Dovich approximation and expressing everything in the Lagrangian frame (i.e. comoving), the angular momentum becomes

$$\boldsymbol{L} = \rho_0 a^5 \int_{V_L} \mathrm{d}^3 q\, (\boldsymbol{q} - \bar{\boldsymbol{q}}) \times \dot{\boldsymbol{x}}, \tag{16}$$

neglecting higher order terms (White 1984; Catelan & Theuns 1996; Crittenden et al. 2001). The velocity $\dot{\boldsymbol{x}}$ is given via the gradient of the potential ψ, which can be expanded in the vicinity of the centre of gravity $\bar{\boldsymbol{q}}$ if its variation across the Lagrangian volume V_L is small:

$$\partial_i \psi(\boldsymbol{q}) \approx \partial_i \psi(\boldsymbol{q})\Big|_{\boldsymbol{q}=\bar{\boldsymbol{q}}} + \partial_{ij}\psi(q)\Big|_{\boldsymbol{q}=\bar{\boldsymbol{q}}} (\boldsymbol{q} - \bar{\boldsymbol{q}})_j, \tag{17}$$

with expansion coefficients $\psi_{ij} \equiv \partial_{ij}\psi$ describing the tidal shear given in equation (12). The first term can be neglected as it only describes the displacement of the protohalo, the second however will be responsible for the rotational effects. Introducing the inertial tensor I_{ij} as

$$I_{ij} = \rho_0 a^3 \int_{V_l} \mathrm{d}^3 q\, (\boldsymbol{q} - \bar{\boldsymbol{q}})_i (\boldsymbol{q} - \bar{\boldsymbol{q}})_j, \tag{18}$$

the angular momentum can be written as

$$L_i = a^2 \dot{D}_+ \epsilon_{ijk} I_{jl} \psi_{lk}, \tag{19}$$

with the Levi–Civita symbol ϵ_{ijk}. The matrix product in the latter expression $\boldsymbol{X} = \boldsymbol{I}\boldsymbol{\Psi}$ can be decomposed into a symmetric $\boldsymbol{X}^+$ and an antisymmetric part $\boldsymbol{X}^-$ defined via the anticommutator and the commutator, respectively:

$$\boldsymbol{X}^+ \equiv \frac{1}{2}\{\boldsymbol{I}, \boldsymbol{\Psi}\}, \quad \boldsymbol{X}^- \equiv \frac{1}{2}[\boldsymbol{I}, \boldsymbol{\Psi}]. \tag{20}$$

With this definition, the angular momentum can be written as (Schäfer 2009; Schäfer & Merkel 2012)

$$L_i = a^2 \dot{D}_+ \epsilon_{ijk} X_{jk} = a^2 \dot{D}_+ \epsilon_{ijk} X^-_{jk}, \tag{21}$$

since the contraction with ϵ_{ijk} will only pick out the antisymmetric part of $\boldsymbol{X}$. Thus, angular momentum is not generated if inertia and tidal shear have a common eigensystem, which is always the case for a matter distribution invariant under SO(3), therefore we need to have $\boldsymbol{X}^- \neq 0$ to generate angular momentum. On the other hand, $\boldsymbol{X}^+$ will measure the alignment of the eigensystems of inertia and shear and thus cause shear effects due to deformations.

The components of the inertial tensor $\boldsymbol{I}$ can be expressed via second derivatives of the density field $\delta(\boldsymbol{x})$ which are given by

$$\delta_{ij} = -\int \frac{\mathrm{d}^3 k}{(2\pi)^3} k_i k_j \delta(\boldsymbol{k}) \exp(\mathrm{i}\boldsymbol{k}\boldsymbol{x}). \tag{22}$$

Thus, the decomposition works in the same way as before:

$$\begin{aligned}
\sigma_2 y^0_{20} &= \sqrt{5/4}\left(\delta_{xx} + \delta_{yy} - \delta_{zz}\right), \\
\sigma_2 y^0_{2\pm1} &= \sqrt{15/2}\left(\delta_{xz} \pm \mathrm{i}\delta_{yz}\right), \\
\sigma_2 y^0_{2\pm2} &= \sqrt{15/8}\left(\delta_{xx} - \delta_{yy} \pm 2\mathrm{i}\delta_{xy}\right), \\
\sigma_2 y^1_{00} &= (\delta_{xx} + \delta_{yy} + \delta_{zz}).
\end{aligned} \tag{23}$$

At a peak in the density field, the peak slope is approximated by a parabolic function

$$\delta(\boldsymbol{x}) = \boldsymbol{x}_p - \frac{1}{2}\lambda_i (\boldsymbol{x} - \boldsymbol{x}_p)_i^2, \tag{24}$$

with the eigenvalues λ_i of the mass tensor $m_{ij} = -\delta_{ij}$ at the peak. If the boundary of the peak is given by the isodensity contour with $\delta = 0$, the inertia tensor can be written as

$$\boldsymbol{I} = \frac{\eta_0}{5}\Gamma \mathrm{diag}\left(A_y^2 + A_z^2, A_x^2 + A_z^2, A_x^2 + A_y^2\right), \tag{25}$$

in the eigensystem of the paraboloid. Here, $A_i = \sqrt{2\delta/\lambda_i}$ are the ellipsoids semi-axes, Γ its volume and η_0 its density, such that $M = \eta_0\Gamma$ is the mass of the peak. In our approximation, the density field is assumed to be homogeneous to the first order, and thus $\eta_0 = \Omega_\mathrm{m}\rho_\mathrm{crit}a^3$. We thus sample values for $\boldsymbol{X}^\pm$ from the joint covariance matrix of δ_{ij} and ψ_{ij}. All calculations are carried out in the eigensystem of the inertia tensor, i.e. we sample values y^n_{lm} and calculate the inertia tensor by inverting equation (23) and using equation (25).

3.4 Decomposition of the shear tensor

In the last two parts, we described how the statistics of the density field induce tidal gravitational fields, encoded in $\boldsymbol{\Psi}$, and how these tidal fields can give rise to rotation. Since the shear effects are as well described by the tidal tensor, the scope of this section will be to decompose $\boldsymbol{\Psi}$ into two separate parts whose invariants can be identified with σ^2 and ω^2. Physically, the shear corresponds to convergent flows, which will deform the halo, while the rotational part will give rise to an overall spinning of the halo induced by the external fields. As already mentioned, angular momentum will only be sourced by the antisymmetric part of the matrix product $\boldsymbol{X}$; the Hodge dual to the angular momentum is the tensor

$$L_{ij} = a^2 \dot{D}_+ [\boldsymbol{I}, \boldsymbol{\Psi}]_{ij}. \tag{26}$$

Now, since the angular momentum can also be expressed as

$$L_i = I_{ij}\omega_j, \tag{27}$$

with angular velocity ω_j, we can conclude that

$$L_{ij} = I_{il}\omega_{lj}, \tag{28}$$

and thus, in matrix–vector notation

$$\boldsymbol{\omega} = \boldsymbol{I}^{-1}\boldsymbol{X}^-. \tag{29}$$

For the shear, we proceed in complete analogy, but using the anti-commutator instead of the commutator. In particular, we decompose the tidal gravitational field as follows:

$$\boldsymbol{\Psi} = \boldsymbol{I}^{-1}\boldsymbol{I}\boldsymbol{\Psi} = \boldsymbol{I}^{-1}\boldsymbol{X}^+ + \boldsymbol{I}^{-1}\boldsymbol{X}^- \equiv \tilde{\boldsymbol{\sigma}} + \tilde{\boldsymbol{\omega}}. \tag{30}$$

Here, we identified the shear tensor $\tilde{\boldsymbol{\sigma}}$ and the rotation tensor $\tilde{\boldsymbol{\omega}}$. Since $\tilde{\boldsymbol{\sigma}}$ still carries a trace, we need to subtract it to arrive at the following expressions for the shear tensor and rotation tensor, respectively:

$$\boldsymbol{\sigma} = \frac{1}{2}\left(\boldsymbol{\Psi} + \boldsymbol{I}^{-1}\boldsymbol{\Psi}\boldsymbol{I}\right) - \frac{\mathrm{tr}\boldsymbol{\Psi}}{3}\mathbb{I}_3, \quad \boldsymbol{\omega} = \frac{1}{2}\left(\boldsymbol{\Psi} - \boldsymbol{I}^{-1}\boldsymbol{\Psi}\boldsymbol{I}\right). \tag{31}$$

The interpretation of the two expressions is straightforward: $\boldsymbol{\sigma}$ measures the alignment between the eigenframes of the tidal tensor and the inertial tensor, while $\boldsymbol{\omega}$ measures their misalignment. Clearly, if both are completely aligned, the tidal tensor will not induce any rotation and only the shear effect is present. If, however, the two frames are not aligned, the inertial tensor will start rotating into the frame of the tidal tensor and keep its rotation once the lever arm will reduce dramatically during collapse.

Downloaded from https://academic.oup.com/mnras/article-abstract/473/4/4558/4411833
by University of Manchester user
on 30 November 2017

3.5 Model comparison

Having set up all the important relations, it is worthy to compare the models presented here with the one from R16 and the phenomenological model in Del Popolo et al. (2013a,b).

The procedure of R16 is quite similar to the one outlined here. Values for the tidal tensor $\boldsymbol{\Psi}$ are sampled in the same way, the values for the inertial tensor, however, are not sampled from the density field and $\boldsymbol{I}$ is implicitly assumed to be the one of the spherical objects. $\boldsymbol{I}$ is thus proportional to the identity, which itself commutes with every other tensor, thus setting $\boldsymbol{\omega}$ to zero identically. Especially, this means equation (31) was

$$\boldsymbol{\sigma} = \boldsymbol{\Psi} - \frac{\mathrm{tr}\boldsymbol{\Psi}}{3}\mathbb{I}_3\,, \quad \boldsymbol{\omega} = 0, \tag{32}$$

for the model presented in R16, and thus the inertial tensor is not needed as well as the condition to consider peaks in the density field only. This leads to a few subtle differences between the two models in terms of the physical interpretation: Both models describe the collapse of a spherically symmetric test object in a Gaussian random field. In both cases, the tidal tensor $\boldsymbol{\Psi}$ is evaluated from the statistics of the underlying linearly evolved density field and gives rise to effective external forces that act on the collapse equation as an inhomogeneity. While the position of the test mass in R16 has been arbitrary, we restrict ourselves to peaks in the density field here and include the possible spin-up due to tidal torquing of the test mass. The restriction to peaks in the density field will generally lead to higher values in $\boldsymbol{\Psi}$ compared to R16, due to the non-trivial correlation with $\boldsymbol{I}$. In this sense, the model presented here is more realistic, in terms of the shear and rotation being just inhomogeneities entering in the collapse equation, than the one in R16.

The comparison with Del Popolo et al. (2013b) is somewhat more difficult as their model was heuristically motivated only. In contrast, our model relies on the statistics of the cosmic density field only and is in this sense only restricted by the validity of Lagrangian perturbation theory at the first order. This is certainly valid as long as $\delta \ll 1$. If we are considering objects with masses above $10^14\,\mathrm{M}_\odot$, this criterion is certainly satisfied in the sense of that the variance of the density field smoothed at this scale is well below unity. In particular, Del Popolo et al. (2013b) find values for $\omega^2 > \sigma^2$ which is not possible with our treatment. This is because in Del Popolo et al. (2013b), the rotation term was derived to match the angular momentum of galaxies and clusters today, being therefore a non-linear quantity. This value will be exceeding our estimate of the rotation tensor and lead to effects that are opposite to what we find.

3.6 Calculation of the invariant $\sigma^2 - \omega^2$

The invariant quantities σ^2 and ω^2 just differ by the sign of the cross terms and by the terms which arise due to the term including the trace of $\boldsymbol{\Psi}$. It is easy to see that the latter terms vanish identically, and thus the only difference between σ^2 and ω^2 is the sign of the two cross terms, which are themselves identical due to the cyclicity of the trace. Generalizing this reasoning to higher order invariants in a coordinate free way, we use that the invariants correspond to the Frobenius norm of the tidal tensor and the inertia tensor. The Frobenius norm of a symmetric matrix $\mathbf{A}$ is defined as

$$||\mathbf{A}||^2 := \mathrm{tr}\mathbf{A}^2 \equiv A_{ij}A^{ji}. \tag{33}$$

An inner product can be defined in the following way

$$\langle \mathbf{A}, \mathbf{B}\rangle = \mathrm{tr}\mathbf{A}\mathbf{B} = A_{ij}B^{ji}, \tag{34}$$

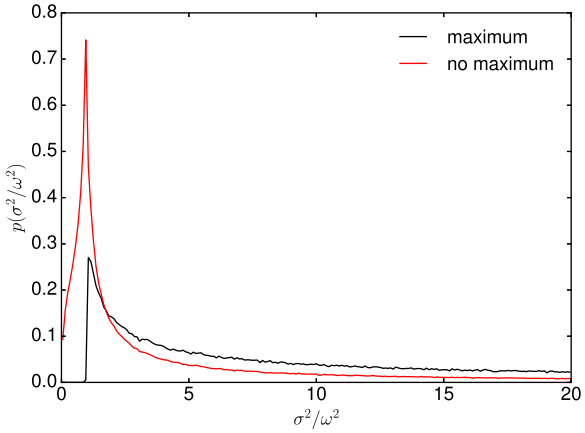

Figure 1. Distributions of the ratio of the two invariants σ^2 and ω^2. The red histogram does not include the maximum constraint, i.e. $\lambda_i > 0$, while the black histogram includes this constraint. Clearly the constraint moves all values that would have $\sigma^2 < \omega^2$ to values $\sigma^2 > \omega^2$ as it is expected from the analytical considerations made in equation (35). The smoothing length for the power spectrum is $R = 10\,\mathrm{Mpc}h^{-1}$.

which is also called Frobenius scalar product, and then inducing the Frobenius norm defined above. With this, we find

$$\begin{aligned}\sigma^2 &= ||\{\boldsymbol{I}, \boldsymbol{\Psi}\}||^2 = ||\boldsymbol{I}\boldsymbol{\Psi}||^2 + 2\langle \boldsymbol{I}\boldsymbol{\Psi}, \boldsymbol{\Psi}\boldsymbol{I}\rangle + ||\boldsymbol{\Psi}\boldsymbol{I}||^2\\ \omega^2 &= ||[\boldsymbol{I}, \boldsymbol{\Psi}]||^2 = ||\boldsymbol{I}\boldsymbol{\Psi}||^2 - 2\langle \boldsymbol{I}\boldsymbol{\Psi}, \boldsymbol{\Psi}\boldsymbol{I}\rangle + ||\boldsymbol{\Psi}\boldsymbol{I}||^2.\end{aligned} \tag{35}$$

Clearly, the positive definiteness of the Frobenius norm implies that $\sigma^2 > \omega^2$ is fulfilled if $\langle \boldsymbol{I}\boldsymbol{\Psi}, \boldsymbol{\Psi}\boldsymbol{I}\rangle > 0$. Due to the cyclic property of the trace, this term can be shown to be $\langle \boldsymbol{I}\boldsymbol{\Psi}, \boldsymbol{\Psi}\boldsymbol{I}\rangle = \mathrm{tr}(\boldsymbol{I}\boldsymbol{\Psi}^2\boldsymbol{I}) = \mathrm{tr}(\boldsymbol{I}^2\boldsymbol{\Psi}^2) = \langle \boldsymbol{I}^2, \boldsymbol{\Psi}^2\rangle$, which in turn is positive for positive (semi)definite matrices $\boldsymbol{I}$ and $\boldsymbol{\Psi}$.

To show this, one can use the generalization of the inequality of the arithmetic and geometric mean,

$$\frac{1}{n}\langle \boldsymbol{I}^2, \boldsymbol{\Psi}^2\rangle = \frac{1}{n}\mathrm{tr}(\boldsymbol{I}^2\boldsymbol{\Psi}^2) \geq (\det(\boldsymbol{I})\det(\boldsymbol{\Psi}))^{\frac{2}{n}} \geq 0, \tag{36}$$

which is only valid for positive (semi)definite matrices, with n being the dimension of the matrices. The tidal shear is positive definite at a peak of the density field, because $\mathrm{tr}(\boldsymbol{\Psi}) = \Delta\Psi = \delta > 0$ due to the Poisson equation, and the inertia can only sensibly be defined at a maximum of the density field, where the curvature of the density field assumes positive values, resulting in a positive definite inertia $\mathrm{tr}(\boldsymbol{I}) > 0$. The argumentation applies for the traceless shear as well, as a positive semidefinite matrix. Both determinants are positive for positive definite matrices, and constrain the scalar product $\langle \boldsymbol{I}^2, \boldsymbol{\Psi}^2\rangle$ to be larger than zero. This is an important result, and we find that the induced shear is always larger than the induced rotation by tidal torquing.

Fig. 1 shows the effect mentioned in equation (35) very clearly: If we restrict the random process to maxima in the density field all values with $\sigma^2 < \omega^2$ disappear and get shifted to larger ratios of σ^2/ω^2. Thus, gravitational tidal fields will always introduce more shear than rotation by tidal torquing if only maxima of the underlying density field are considered. This is indeed a necessary condition, since otherwise the inertia tensor would not be defined in a proper way. As a consequence, the collapse will always proceed faster in a scenario with tidal gravitational fields than in a uniform background as it is the case for the SPC.

We show the, not normalized, joint distribution of σ^2 and δ in Fig. 2. Due to the correlations in the y^n_{lm} basis given in equation (13), the maximum constraint enforces higher values in

Downloaded from https://academic.oup.com/mnras/article-abstract/473/4/4558/4411833
by University of Manchester user
on 30 November 2017

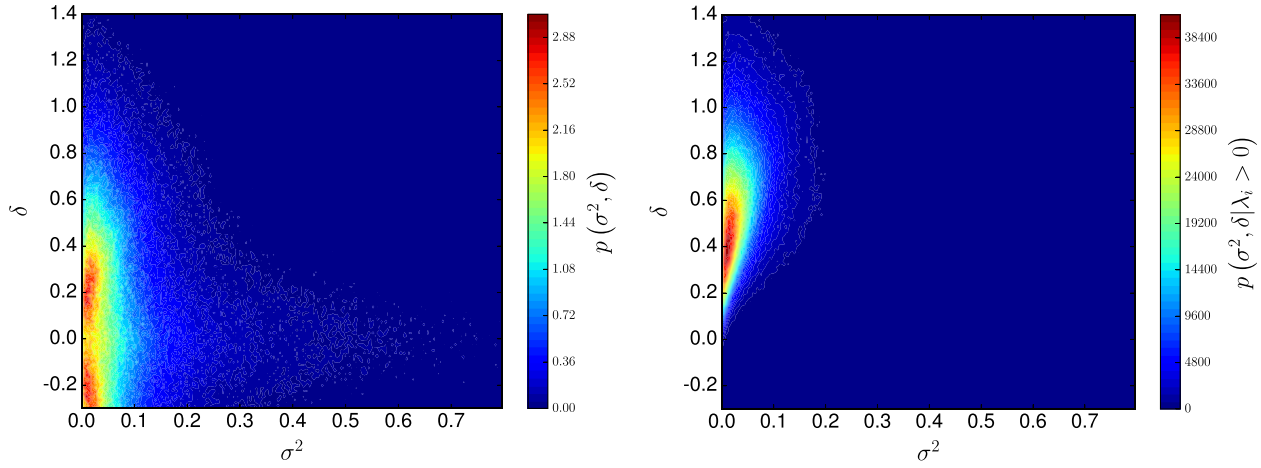

Figure 2. Joint distributions (not normalized) of the density contrast $\delta = \mathrm{tr}(\Psi)$ and the invariant σ^2. Left-hand panel: no maximum constraint. The distribution is similar to the distribution found in R16. Right-hand panel: the maximum constraint is imposed. Clearly the constraint enforces higher values of δ and thus also in σ^2, which is due to the correlations in the y^n_{lm} basis given in equation (13). The smoothing length for the power spectrum is $R = 10\,\mathrm{Mpc}h^{-1}$.

δ and σ^2. In particular, peaks can only be found if $\delta > 0$, which is indeed necessary to write down the inertia tensor as in equation (25), as the ellipsoid is a region with a boundary $\delta = 0$. Also, the density peaks are significantly higher than without the constraint.

In Fig. 3, we show the distribution of $\sigma^2 - \omega^2$ with different thresholds for the overdensity δ at the peak. Clearly, higher overdensities at the peak imply higher shear values as the potential is more curved at higher peaks.

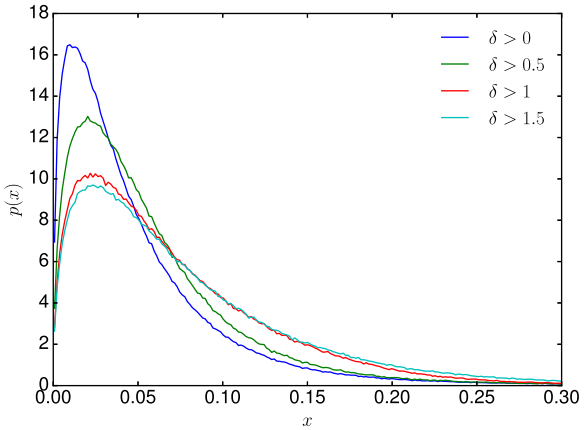

Figure 3. Distributions of the invariants $\sigma^2 - \omega^2$ for different thresholds δ on a scale of $R = 10$ Mpch^{-1}. Higher peaks induce higher values for $\sigma^2 - \omega^2$.

4 INFLUENCE ON δ_c, Δ_V AND SCALING PROPERTIES

In this section, we investigate the influence of the tidal gravitational fields on the collapse dynamics by substituting the invariants σ^2 and ω^2 into the collapse equation. Additionally, we will study the scaling with the mass of the collapsed structure. The cosmology is chosen to be a concordance ΛCDM model with $\Omega_\mathrm{m} = 0.3$, $\Omega_\Lambda = 0.7$, $w = -1$, $h = 0.7$, $\sigma_8 = 0.8$ and $n_\mathrm{s} = 0.96$.

In Fig. 4, the resulting distribution of δ_c is shown. The collapse always proceeds faster than in the case without tidal fields. For more work on this, we refer to Hoffman (1986), Zaroubi & Hoffman (1993) and Bertschinger & Jain (1994). As discussed in the previous section, this is due to the fact that the tidal field induced shear is always higher than the effect due to tidal torquing, provided we restrict our considerations to maxima in the density field. Thus, the strong drop of the distribution at higher δ_c marks the value that one would get within a uniform background.

Due to the faster collapse, virialized objects form more easily, thus yielding more massive objects. This effect is similar to modified gravities theories or dark energy cosmologies with non-phantom equations of state. Since the distribution found for δ_c is similar to the one found in R16 and no significant differences were found for more complex dark energy models, we refer to our previous works regarding the impact on the mass function and cluster counts (see Reischke et al. 2016a; Pace et al. 2017).

δ_c exhibits a mass dependence due to the low-pass filter with a scale R which is introduced to model the effective tidal fields acting on an object of size $R(M)$. We consider again the averaged values of the invariant $\sigma^2 - \omega^2$ or the linear critical density contrast δ_c, i.e. given the distribution $p(\delta_\mathrm{c})$ we consider

$$E[\delta_\mathrm{c}] = \int p(\delta_\mathrm{c})\delta_\mathrm{c}\mathrm{d}\delta_\mathrm{c}, \tag{37}$$

and similarly for $\sigma^2 - \omega^2$. On the left-hand panel in Fig. 5, we show the scaling of $E[\sigma^2 - \omega^2]$ with respect to the mass. The general scaling shows that higher masses result into lower values for $\sigma^2 - \omega^2$ as larger objects are only influenced by low-frequency modes that become smaller for increasing scale. In the case considered here, we restrict ourselves to maxima in the density field, and thus the situation is constructed such that the curvature of the density field must be negative, yielding slightly more shear on large scales than for a random point in the density field. On smaller scales, however, the situation is reversed. This argument is precisely due to the additional factor k^4 which enters in the random process for δ_{ij} (cf. equations 11 and 23).

The right-hand panel of Fig. 5 shows the resulting scaling of $E[\delta_\mathrm{c}]$. Here, we additionally show the constant value (green curve) obtained without gravitational tidal fields. As for the invariants σ^2 and ω^2 the qualitative behaviour is identical. We find that the term $\sigma^2 - \omega^2$ will always favour the collapse, thus lowering $E[\delta_c]$. Even though ω^2 will act against the collapse, as it corresponds to a centrifugal force, it can never dominate σ^2 as we showed before. For completeness, we note that our final results for $E[\delta_\mathrm{c}]$ are effectively very similar to the ones found in R16. Furthermore, we note that the time evolution of the invariant is controlled by the time derivative of the growth factor introduced in equation (8) and is

Downloaded from https://academic.oup.com/mnras/article-abstract/473/4/4558/4411833
by University of Manchester user
on 30 November 2017

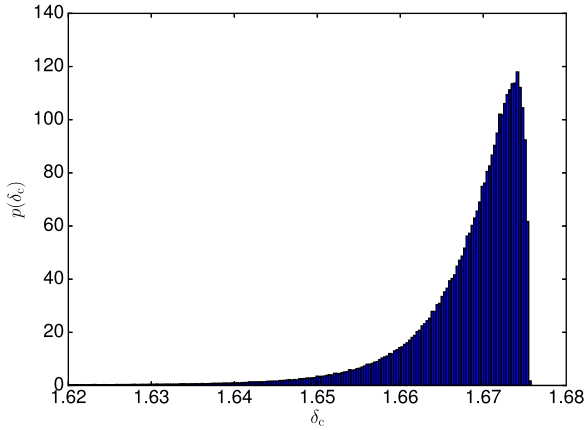

Figure 4. Distribution of the critical linear overdensity δ_c for a standard ΛCDM cosmology. The smoothing scale is again $R = 10\ \mathrm{Mpc}h^{-1}$ and the density threshold is $\delta = 0$.

thus purely due to background dynamics. If one instead starts with a non-spherical collapse, one would find larger effects on δ_c compared to this idealized model. An example for this is the ellipsoidal collapse model (Eisenstein & Loeb 1995; Ohta et al. 2003, 2004; Angrick & Bartelmann 2010), where δ_c values are normally substantially higher than for the spherical collapse case, especially at low redshift and mass.

A very important and interesting quantity that can be evaluated within the framework of the spherical collapse model is the virial overdensity Δ_V, representing the overdensity of the collapsing object at the virialization epoch (see also Meyer, Pace & Bartelmann 2012, for a discussion of this quantity in a general relativistic setting). The virial overdensity is also related to the size of spherically symmetric haloes and its value can be inferred by embedding the virial theorem into the formalism. When including the shear and rotation terms into the equations of motion for dark matter perturbations, Δ_V becomes, in analogy to δ_c, mass-dependent. However, one finds that Δ_V is practically independent of mass and it evolves as if the system is evolving in an ideal background, i.e. without shear and rotation. This is an interesting result but not unexpected. As showed in R16, the virial overdensity is insensitive to mass since the quantities involved for its determination are evaluated still in the linear regime and perturbations with respect to the spherically symmetric case are of the order of per mill. Taking also into account that rotation has always a smaller contribution than the shear and their combined effect makes the rotating ellipsoid closer to the sphere in terms of the perturbation quantities, it is easy to understand why the feature found in R16 still holds.

5 CONCLUSION AND DISCUSSION

In this paper, we extended the work by R16 to estimate the effect of shear and rotation on the spherical collapse of dark matter haloes. The model assumes that the spherical collapse dynamics are only altered in terms of an inhomogeneity in the collapse equation which also only enters in the non-linear equation. In this sense, the model describes the spherical collapse of a test mass in a tidal gravitational field.

By jointly considering the gravitational tidal field and the curvature of the density field, we separated its action into a symmetric traceless part and an antisymmetric part which correspond to the shear tensor and rotation tensor, respectively. These tensors were used to construct the invariants σ^2 and ω^2 in the collapse equation. Physically, the protohalo, forming at the location of a peak, feels the surrounding tidal gravitational field and thus shear effects as well as rotation induced by tidal torquing. This procedure is identical to the one presented in R16 if we restrict our considerations again to peaks with a spherical symmetry. Our findings are the following.

(i) The invariant quantity ω^2 of the rotational part of the tidal tensor is always smaller than the shear invariant σ^2 within the framework of tidal torquing. This statement is not of statistical nature, and it is true for every sample individually.

(ii) The critical linear overdensity δ_c is now a mass-dependent quantity changing by roughly a per cent with respect to the usual spherical collapse value. The overall effect is small at masses below $10^{15}\ \mathrm{M}_\odot$ and completely negligible for masses above.

(iii) External tidal fields will always help objects to collapse into virialized structures even if a rotational term due to tidal torquing is considered. In terms of observations of cluster counts, tidal fields can, in principle, always be confused with dynamical dark energy increasing the abundance of heavy clusters in a purely spherically symmetric case where no tidal fields are taken into account. For a more detailed discussion on this, we refer the reader to R16.

(iv) Comparing this work with Del Popolo et al. (2013a), we find that the deviations of δ_c found there are mainly due to the rotational

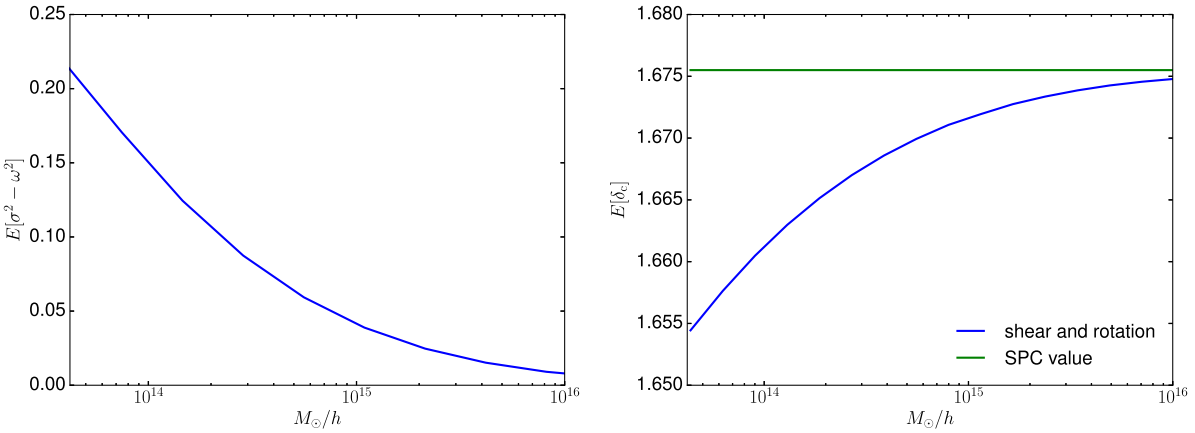

Figure 5. Scaling relations of averaged quantities with mass evaluated at redshift zero. The blue curve shows the effect derived in this paper by including both σ^2 and ω^2. The influence of gravitational tidal fields is highest for low masses, and thus δ_c is also influenced most at the low-mass tail. Left: averaged invariants, right: averaged δ_c. The value for the SPC for a ΛCDM universe is shown in green.

Downloaded from https://academic.oup.com/mnras/article-abstract/473/4/4558/4411833
by University of Manchester user
on 30 November 2017

term, which can become rather large, and thus the collapse is mostly slowed down. Our work finds an opposite result as the gravitational tidal fields always speed up the collapse and the rotational term is nearly negligible. This is, however, also a property of the model we used here. Our model is self-consistent as long as we only consider external tidal effects on a spherically symmetric object where the deformation is negligible compared to the total extent of the collapsing object. In this work, we assumed the halo to be non-spherical prior to collapse to allow it to spin-up as long as the lever arms are large enough. As soon as collapse starts, the collapse is again treated as being spherical. We therefore have a situation in which a spherical overdensity is rotating at an angular speed ω^2 gained by tidal torquing as if it would have been an ellipsoidal object. These limitations make a direct comparison with Del Popolo et al. (2013a) difficult. See point (v) for an explanation based on the way the invariant $\sigma^2 - \omega^2$ is evaluated.

(v) In our self-consistent model, the shear and rotation terms have little effect and their effect grows with time and mass as structures evolve. In the formalism outlined, the invariant $\sigma^2 - \omega^2$ is evaluated at early times when structures are in the linear regime. This explains why, for example, the virial overdensity Δ_V is barely affected. In previous works on the subject (Del Popolo et al. 2013a,b; Pace et al. 2014b) instead, the term $\sigma^2 - \omega^2$ assumes objects to be still spherical in average and that the rotation term matches the present-day rotational velocity of clusters as a function of their mass. This late time evaluation makes the rotation term ω^2 the dominant one and this explains the different trends in the two series of papers.

ACKNOWLEDGEMENTS

RR acknowledges funding by the graduate college 'Astrophysics of cosmological probes of gravity' by Landesgraduiertenakademie Baden-Württemberg. FP is supported by the STFC post-doctoral fellowship with grant R120562 'Astrophysics and Cosmology Research within the JBCA 2017-2020' and thanks Inga Cebotaru for reading the manuscript and providing useful comments. The authors thank an anonymous referee for improving the manuscript.

REFERENCES

Abramo L. R., Batista R. C., Liberato L., Rosenfeld R., 2007, J. Cosmology Astropart. Phys., 11, 12
Abramo L. R., Batista R. C., Rosenfeld R., 2009, J. Cosmology Astropart. Phys., 7, 40
Angrick C., Bartelmann M., 2009, A&A, 494, 461
Angrick C., Bartelmann M., 2010, A&A, 518, A38
Avila-Reese V., Firmani C., Hernández X., 1998, ApJ, 505, 37
Bernardeau F., 1994, ApJ, 433, 1
Bertschinger E., 1985, ApJS, 58, 39
Bertschinger E., Jain B., 1994, ApJ, 431, 486
Catelan P., Theuns T., 1996, MNRAS, 282, 436
Cole S. et al., 2005, MNRAS, 362, 505
Copeland E. J., Sami M., Tsujikawa S., 2006, Int. J. Mod. Phys. D, 15, 1753
Crittenden R. G., Natarajan P., Pen U.-L., Theuns T., 2001, ApJ, 559, 552
Del Popolo A., Pace F., Lima J. A. S., 2013a, Int. J. Mod. Phys. D, 22, 50038
Del Popolo A., Pace F., Lima J. A. S., 2013b, MNRAS, 430, 628
Diego J. M., Majumdar S., 2004, MNRAS, 352, 993
Eisenstein D. J., Loeb A., 1995, ApJ, 439, 520
Fang W., Haiman Z., 2007, Phys. Rev. D, 75, 043010
Fillmore J. A., Goldreich P., 1984, ApJ, 281, 1
Gunn J. E., Gott J. R., III, 1972, ApJ, 176, 1
Heavens A. F., Sheth R. K., 1999, MNRAS, 310, 1062
Hoffman Y., 1986, ApJ, 308, 493
Komatsu E. et al., 2011, ApJS, 192, 18
Lin C.-A., Kilbinger M., 2014, Proc. IAU Symp. 306, Statistical Challenges in 21st Century Cosmology. Kluwer, Dordrecht, p. 107
Majumdar S., 2004, Pramana, 63, 871
Maturi M., Angrick C., Pace F., Bartelmann M., 2010, A&A, 519, A23
Maturi M., Fedeli C., Moscardini L., 2011, MNRAS, 416, 2527
Meyer S., Pace F., Bartelmann M., 2012, Phys. Rev. D, 86, 103002
Mota D. F., van de Bruck C., 2004, A&A, 421, 71
Ohta Y., Kayo I., Taruya A., 2003, ApJ, 589, 1
Ohta Y., Kayo I., Taruya A., 2004, ApJ, 608, 647
Pace F., Waizmann J.-C., Bartelmann M., 2010, MNRAS, 406, 1865
Pace F., Moscardini L., Crittenden R., Bartelmann M., Pettorino V., 2014a, MNRAS, 437, 547
Pace F., Batista R. C., Del Popolo A., 2014b, MNRAS, 445, 648
Pace F., Reischke R., Meyer S., Schäfer B. M., 2017, MNRAS, 466, 1839
Padmanabhan T., 1996, Cosmology and Astrophysics Through Problems. Cambridge Univ. Press, Cambridge
Perlmutter S. et al., 1999, ApJ, 517, 565
Planck Collaboration XIII, 2016, A&A, 594, A13
Regős E., Szalay A. S., 1995, MNRAS, 272, 447
Reischke R., Pace F., Meyer S., Schäfer B. M., 2016a, MNRAS, 463, 429 (R16)
Reischke R., Maturi M., Bartelmann M., 2016b, MNRAS, 456, 641
Riess A. G. et al., 1998, AJ, 116, 1009
Ryden B. S., Gunn J. E., 1987, ApJ, 318, 15
Schäfer B. M., 2009, Int. J. Mod. Phys. D, 18, 173
Schäfer B. M., Koyama K., 2008, MNRAS, 385, 411
Schäfer B. M., Merkel P. M., 2012, MNRAS, 421, 2751
Sunyaev R. A., Zeldovich I. B., 1980, ARA&A, 18, 537
White S. D. M., 1984, ApJ, 286, 38
Zaroubi S., Hoffman Y., 1993, ApJ, 416, 410
Zel'Dovich Y. B., 1970, A&A, 5, 84

This paper has been typeset from a TEX/LATEX file prepared by the author.

Downloaded from https://academic.oup.com/mnras/article-abstract/473/4/4558/4411833
by University of Manchester user
on 30 November 2017